Elucidation of orbital moment, anisotropy, and magnetic damping in epitaxial Fe$_3$O$_4$ films

C. Love,[1,2] J. E. Beevers,[1] B. Achinuq,[1] R. Fan,[2] K. Matsuzaki ●,[3] T. Susaki,[4,5] V. K. Lazarov,[1] S. S. Dhesi,[2] G. van der Laan ●,[2] and S. A. Cavill[1,2,*]

[1]*Department of Physics, University of York, York YO10 5DD, United Kingdom*
[2]*Diamond Light Source, Harwell Science and Innovation Campus, Didcot OX11 0DE, United Kingdom*
[3]*Research Institute for Advanced Electronics and Photonics, National Institute of Advanced Industrial Science and Technology, Tsukuba, Ibaraki 305-8568, Japan*
[4]*Science & Innovation Center, Mitsubishi Chemical Corporation, 1000 Kamoshida-cho, Aoba-ku, Yokohama-shi, Kanagawa 227-8502, Japan*
[5]*Secure Materials Center, Materials and Structures Laboratory, Tokyo Institute of Technology, 4259 Nagatsuta, Midori-ku, Yokohama 226-8503, Japan*

The size of the orbital moment in Fe$_3$O$_4$ has been the subject of a long-standing and contentious debate. In this paper, we make use of ferromagnetic resonance (FMR) spectroscopy and x-ray magnetic circular dichroism (XMCD) to provide complementary determinations of the size of the orbital moment in "bulklike" epitaxial Fe$_3$O$_4$ films grown on yttria-stabilized zirconia (111) substrates. Annealing the 100 nm as-grown films to 1100 °C in a reducing atmosphere improves the stoichiometry and microstructure of the films, allowing for bulklike properties to be recovered as evidenced by x-ray diffraction and vibrating sample magnetometry. In addition, in-plane angular FMR spectra exhibit a crossover from a fourfold symmetry to the expected sixfold symmetry of the (111) surface, together with an anomalous peak in the FMR linewidth at ~10 GHz; this is indicative of low Gilbert damping in combination with two-magnon scattering. For the bulklike annealed sample, a spectroscopic splitting factor $g \approx 2.18$ is obtained using both FMR and XMCD techniques, providing evidence for the presence of a finite orbital moment in Fe$_3$O$_4$.

I. INTRODUCTION

The interest in half-metal materials, which are predicted to be 100% spin-polarized at the Fermi level, has been a major driver in spintronic research over the past decade [1]. Fe$_3$O$_4$ is the archetypal half-metal material due to its predicted 100% polarization at the Fermi level, high Curie temperature ($T_C = 858$ K), and good epitaxial match to technologically important semiconductors and oxides (e.g., GaAs, MgO, and Al$_2$O$_3$), yet the promise of a fully spin-polarized Fermi level has not been realized. Achieving a fully ordered high-quality Fe$_3$O$_4$ thin film is essential for spintronic device applications, and a number of studies have been devoted to growth optimization in order to achieve this. However, the problem with thin-film magnetite is that it tends to show non-bulk-like magnetoresistance (MR) and presents high saturation fields regardless of the film growth technique [2]. The difficulty in magnetically saturating these films has been associated with the presence of anti-phase boundaries (APBs) between ferrimagnetic domains. These have been invoked to explain the large negative magnetoresistance observed in Fe$_3$O$_4$ [3]. In line with the Goodenough-Kanamori-Anderson rules [4], Fe–O–Fe bond angles close to 180°, induced by APBs, give rise to superexchange interactions coupling the adjacent domains antiferromagnetically. The existence of APBs has been extensively reported in the literature and the anomalous thin-film properties correlated to the APB atomic structure and density [5,6]. To improve the structural ordering of the Fe$_3$O$_4$ thin films and reduce the APB density, postannealing in a CO/CO$_2$ atmosphere has been successfully employed [7] and shown to correlate with near bulklike magnetotransport properties.

In this paper, we demonstrate that CO/CO$_2$ annealed films recover bulklike magnetic properties including the expected anisotropy for the (111) geometry. For the annealed sample, the magnetic damping is still dominated by two-magnon scattering (TMS), which is indicative of magnetic inhomogeneities. In particular, a peak in the linewidth as a function of frequency is observed in the FMR data which has only been previously seen in spherical samples [8] or samples with small intrinsic Gilbert damping in combination with TMS [9]. We show than this nonmonotonic behavior is consistent with a small out-of-plane tilting of the magnetization in combination with TMS. Finally, using the two complementary techniques of XMCD and FMR, we unequivocally establish that a finite orbital moment exists in Fe$_3$O$_4$.

II. METHODS

Nominally 100 nm Fe$_3$O$_4$ films were grown by pulsed laser deposition (PLD) on yttria-stabilized zirconia (YSZ)
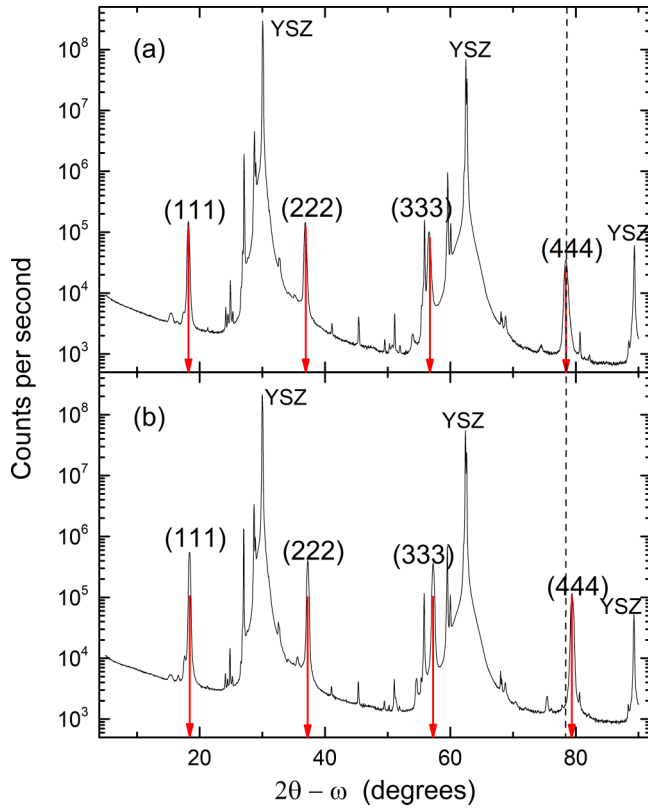
*stuart.cavill@york.ac.uk

FIG. 1. XRD measured in the symmetric geometry for (a) the as-grown sample, and (b) the annealed sample. Red arrows indicate the position of the (hhh) Fe$_3$O$_4$ reflections.

FIG. 2. (a) *M-H* and (b) *M-T* for the as-grown film. (c) *M-H* and (d) *M-T* for the annealed film. *M-H* curves were measured at 300 K. *M-T* curves were measured after field cooling at 30 KOe. The measuring field was set to 1000 Oe.

substrates at 300 °C in a partial oxygen pressure of P_{oxygen} = 2×10^{-4} Pa. Postannealing was performed on one of the films at 1100 °C for 60 min in a CO/CO$_2$ atmosphere with a ratio of 1:5000 as detailed in previous studes [7]. XRD measurements were performed using a non-monochromated Cu $K\alpha$ source while the magnetic measurements were performed using a VSM-SQUID and FMR spectrometer [10]. Fe $L_{2,3}$ x-ray absorption spectroscopy (XAS) and XMCD measurements were performed on beamline I06 at the Diamond Light Source [11]. The XAS was measured in normal incidence by total-electron yield (TEY) using the sample drain current.

III. RESULTS

XRD measurements are shown in Fig. 1 for (a) the as-deposited film and (b) the annealed film. In Fig. 1(a), four peaks are indexed to the (hkl) reflections, where $h = k = l$, of the Fe$_3$O$_4$ structure (space group Fd-$3m$, inverse spinel, $a = b = c = 8.396$ Å) with a lattice constant of 8.440(3) Å. The other peaks in the data are substrate reflections due to the unmonochromated beam. Surprisingly, the Fe$_3$O$_4$ film retains the epitaxial relationship with the YSZ(111) substrate with the following crystallographic relationship: YSZ(111) ∥ Fe$_3$O$_4$(111) and YSZ(1−10) ∥ Fe$_3$O$_4$(1−10), even though the lattice mismatch is ≈22%, $|a_{\text{YSZ}}/\sqrt{2} - a_{\text{Fe3O4}}/2\sqrt{2}|/(a_{\text{Fe3O4}}/2\sqrt{2})$; $a_{\text{YSZ}} = 5.12$ Å.

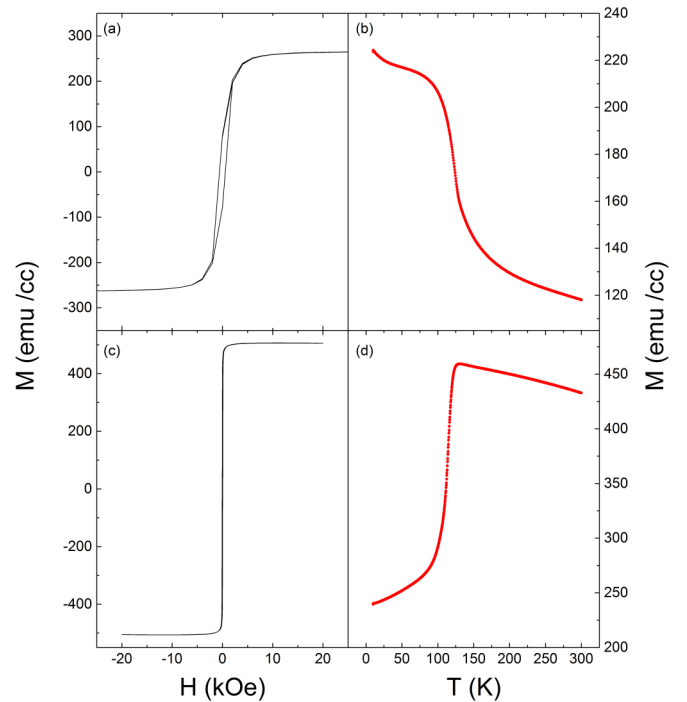Figure 1(b) shows the XRD data for the annealed sample. The same family of (hhh) peaks are present as in the

as-deposited case, retaining the epitaxial relationship to the substrate. However, a clear shift of the reflections to higher angles is seen, giving a smaller lattice constant of 8.355(2) Å compared to the as-deposited case. Upon annealing, the Fe$_3$O$_4$ goes from being compressively strained in the plane of the sample with respect to bulk Fe$_3$O$_4$, to being under tension.

VSM measurements were performed with the applied field parallel to the surface along the [1$\bar{2}$1] direction for temperatures between 5 and 300 K. Figure 2 shows magnetometry data for the as-grown and annealed films. Room-temperature $M(H)$ data are shown in Figs. 2(a) and 2(c) for the as-grown and the annealed films, respectively, while the temperature-dependent magnetization, after field cooling in a saturating field of 30 kOe, is shown in Figs. 2(b) and 2(d). The effect of annealing in the CO/CO$_2$ environment is evident from the increase in saturation magnetization from 260 to ≈470 emu/cm^3, the decrease in coercivity (580–52 Oe), and the increased squareness of the loop (0.3–0.8), which all suggest an improved magnetic structure with bulklike properties. Magnetic structure improvements due to the annealing procedure can also be seen in the field-cooled $M(T)$ data. The as-grown sample magnetization drops rapidly around 100 K before decreasing more gradually at approximately 120 K. Conversely, the annealed sample displays a sharp increase in magnetization around 115 K before gradually decreasing with temperature. Such behavior is typical of bulk magnetite around the Verwey transition temperature, known to be a very sensitive probe of chemical disorder [12].

To gain a detailed understanding of the role of CO/CO$_2$ annealed Fe$_3$O$_4$, XAS/XMCD measurements were performed at the Fe $L_{2,3}$ absorption edges in order to determine the
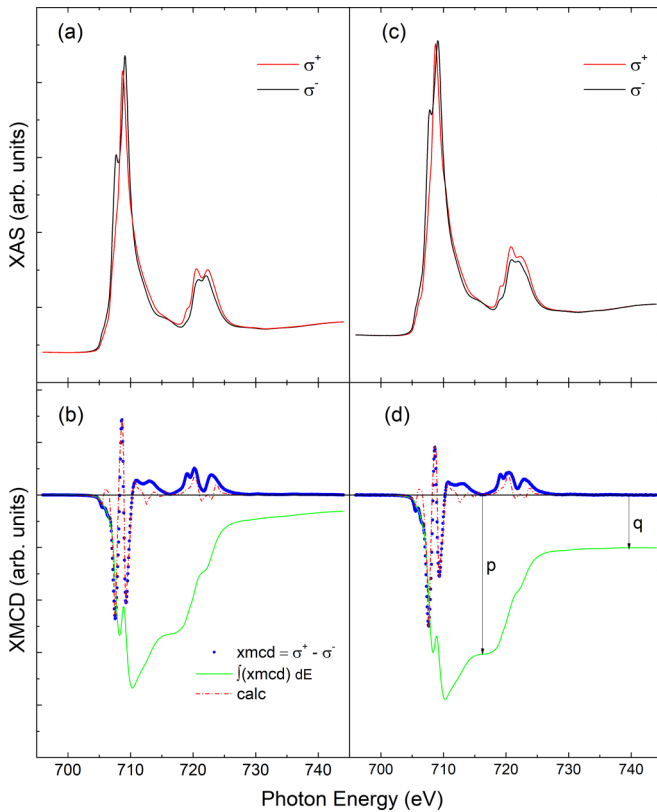
FIG. 3. Circular polarization-dependent XAS at the Fe $L_{2,3}$ edges for (a) the as-grown sample and (c) the annealed sample. XMCD (blue dots) and integrated XMCD (green line) spectra for (b) the as-grown sample and (d) the annealed sample. Atomic multiplet simulations of the XMCD are shown by a red dash-dotted line on top of the experimental XMCD. p is the integral over the L_3 edge, and q is the integral over the L_3 and L_3 edges.

valency, coordination, and magnetic properties of the Fe cations. In L-edge XAS, electrons are excited from a $2p$ core level to the unoccupied $3d$ valence states of the element of interest by circularly polarized x-rays at the resonance energy of the transition. The difference in absorption for opposite chirality of the polarizations (XMCD) gives a direct and element-specific measurement of the projection of the $3d$ magnetic moment along the x-ray helicity vector [13]. The absorption cross section is commonly obtained by measuring the decay products, typically TEY detection, of the photoexcited core hole. The type of decay product measured determines the probing depth of the technique. At the $L_{2,3}$ absorption edges of $3d$ transition metals, the probing depth for TEY detection is approximately 6 nm. All measurements were performed at normal incidence, which reduces the effect of self-absorption on the spectra [14], in a 5 T field applied collinear to the x-ray helicity vector.

Figure 3 shows XAS and XMCD data for the as-grown sample (a,b) and the annealed sample (c,d) at the Fe $L_{2,3}$ edges. The XAS at the Fe $L_{2,3}$ edges for both samples shows multiplet structure typical of iron oxide. Three peaks, two negative and one positive, are present in the XMCD spectra at the L_3 edge, similar to that found in other XMCD studies of Fe_3O_4 [13]. These peaks correspond to contributions from

Fe^{3+} in octahedral (O_h), Fe^{3+} in tetrahedral (T_d), and Fe^{2+} in octahedral sites. For the ferrimagnetic spinel structure, spins located on the T_d sites are aligned antiparallel to the spins on the O_h sites [15]. Hence, the positive peak in the XMCD at the L_3 edge is due to tetrahedrally coordinated Fe^{3+}. Fits to the XMCD data using atomic multiplet calculations [16] show that the XMCD spectra for the as-grown sample are best represented by the ratio for the Fe^{2+} O_h, Fe^{3+} T_d, and Fe^{3+} O_h of 0.8 : 1.05 : 1.05, whereas for the annealed sample a ratio of 1.05 : 1 : 0.95 is obtained. A clear increase in the amount of Fe^{2+} contributing to the magnetic signal is observed upon annealing the sample, consistent with the reducing CO/CO_2 environment and further demonstrating an improved stoichiometry of the film.

Integrating the XMCD spectra and applying the XMCD sum rules [17] provides the spin to orbital magnetic moment ratio. In $3d$ transition metals, the orbital magnetic moment is almost completely quenched by the crystal-field interaction, and so the g-factor is approximately equal to the free-electron value of 2. For small orbital contributions, the g-factor can be expressed as [18]

$$g = 2\left(\frac{\mu_L}{\mu_S} + 1\right), \tag{1}$$

where μ_S and μ_L are the spin and orbital magnetic moment, respectively. The ratio of the orbital to spin magnetic moment can be conveniently obtained from the XMCD sum rules such that [13]

$$\frac{\mu_L}{\mu_S} = \frac{2q}{9p - 6q}, \tag{2}$$

where p and q are the integrated intensities over the L_3 and $L_{2,3}$ XMCD signal, respectively. For the as-grown film we obtain $g = 2.14 \pm (0.01)$, while for the annealed film the XMCD sum rules give $g = 2.18 \pm (0.01)$. As can be seen directly from the integrated XMCD, this is due to a larger orbital moment ($\mu_L \propto q$) for the annealed film ($0.27\,\mu_B$) compared to the as-grown material, consistent with the increase in Fe^{2+} for the former.

A debate on the size of the orbital moment in Fe_3O_4 has been ongoing for the past 15 years. Goering *et al.* [19] measured a vanishingly small orbital moment, while Huang *et al.* [20] measured a large orbital moment of $0.67\,\mu_B$; both studies used high-quality single crystals of Fe_3O_4. Artefacts due to self-absorption in TEY, the extent of the integration range in sum-rule analysis, and site compensation of orbital moments have all been invoked to explain the discrepancy [21]. More recently, quadrupole transitions at the K-edge XMCD of bulk Fe_3O_4 gave an orbital moment of $0.26\,\mu_B$, associated with the formal Fe^{2+} site, in good agreement with our results [22]. The orbital magnetic moment was shown to have a strong dependence on the magnetic-field direction leading to large variations in the measured magnitude, a possible explanation for the observed differences reported in the literature. One implication of a fully quenched orbital moment, as found by Goering *et al* [19], is that $g = 2$, which can easily be verified by FMR spectroscopy. Surprisingly, the data obtained from the two spectroscopic methods (XMCD and FMR) have not been extensively compared for this "model" ferrimagnetic oxide system. Bickford *et al.* [23] measured the g-factor in a
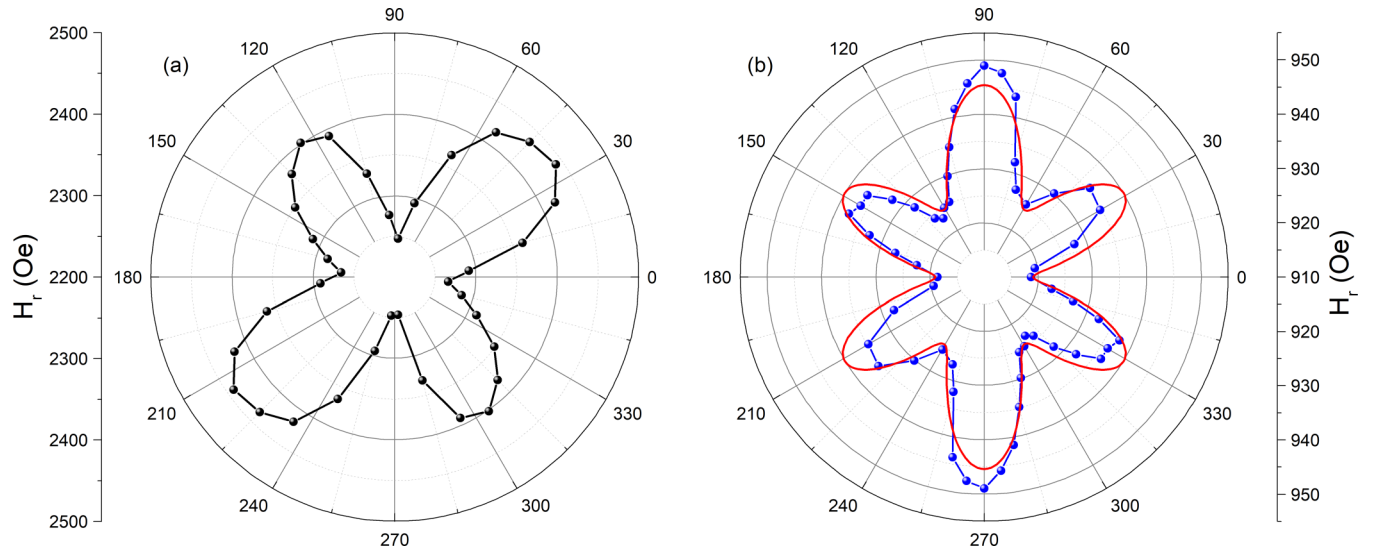
FIG. 4. In-plane (azimuthal) dependence of the FMR resonant field (H_r) measured at 10 GHz for (a) the as-grown film and (b) the film annealed at 1100 °C. The red curve in (b) is a simulated curve generated using Eq. (4) and extracted parameters.

number of bulk Fe_3O_4 samples using angle-dependent FMR, and they obtained a *g*-factor of 2.12 and 2.17 for natural and synthetic samples, respectively. The results of this seminal study strongly suggest a nonzero orbital moment in Fe_3O_4, and they are in good agreement with the *g*-factor obtained by XMCD on the annealed thin-film sample of this current study ($g = 2.18$) and in the recent *K*-edge data of bulk magnetite [22].

To obtain secondary evidence of a nonzero orbital moment via the *g*-factor, angle-resolved FMR spectra were measured for the two samples. For these measurements, a broadband field modulated FMR was utilized in combination with an electromagnet capable of applying a field at any point in a circle of 0.5 T radius. The plane of the sample was aligned with the plane of rotation in order to measure the in-plane magnetic anisotropy.

Field sweeps along different azimuthal angles at a fixed frequency were measured to observe changes in the resonance reflecting the in-plane anisotropy of the samples. Figure 4 shows the in-plane anisotropy for the (a) as-grown and (b) annealed films, respectively. The frequency of excitation was 10 GHz with the applied field (H) at $\phi = 0°$ corresponding to the [1$\bar{2}$1] axis of the sample. The as-grown film displays a distorted fourfold symmetry, while the annealed film shows a combination of sixfold and twofold symmetries. For the annealed film, the measured anisotropy is predominantly cubic with the easy axis along [1$\bar{2}$1]. For cubic magnetic thin films grown on (111) surfaces, the effective demagnetizing field forces the magnetic moment of the system to lie close to the (111) plane, perpendicular to the surface normal. The first-order magnetocrystalline anisotropy (MCA) is along the $\langle 111 \rangle$ direction for negative K_c, with the competition between the MCA and demagnetizing field resulting in a small deviation of the magnetization away from the (111) plane. As a result, the in-plane resonance field should display sixfold symmetry with the in-plane easy axes along the [1$\bar{2}$1] directions for negative K_c. The cubic contribution to the measured anisotropy for a flat (111) film is small, with variations in

the resonance field on the order of a few 10s of Oe [24]. In-plane uniaxial anisotropy should not be present in a pure cubic system. However, a small in-plane uniaxial anisotropy is present in the annealed film, as evidenced by the slightly lower resonance field along [1$\bar{2}$1] compared to the other easy-axis directions. Uniaxial anisotropies on cubic (111) surfaces have also been seen previously where thin films of Fe grown on Si(111) substrates have been shown to display a step edge induced uniaxial anisotropy [25].

The as-grown film shows an intriguing in-plane anisotropy. For a cubic system measured in the (001) plane, a fourfold symmetry, similar to Fig. 4(a), would be expected, with easy axes along the [100] and [010] directions displaying resonant field minima. However, for films grown on YSZ(111) the anisotropy should be sixfold-symmetric. Nonepitaxy with the substrate may relax this condition, yet the XRD data give evidence that the film is (111) oriented. There is no clear explanation for the observed angular dependence of the magnetic resonance, although speculatively this may be a consequence of a small miscut of the substrate leading to a high step edge density and mosaicity of the film. As reported in Ref. [25], small misorientations are sufficient to reduce the sixfold symmetry to a fourfold one, resulting in variations in the resonant field much larger than in the (111) plane, which is what we observe experimentally. Annealing at high temperatures (1100 °C) may smooth the interface, reducing the mosaicity and allowing for a recovery of the sixfold symmetry. We also note that the diffraction intensity of the (*hhh*) Fe_3O_4 reflections is higher after annealing, supporting this hypothesis.

Values of the *g*-factor were obtained by measuring FMR field swept spectra as a function of RF driving frequency in the range 4–20 GHz. FMR ideally measures the imaginary part of the complex magnetic susceptibility, which is best represented by a symmetric Lorentzian line shape. However, FMR line shapes are often asymmetric due to a small mixing of the real and imaginary parts of the magnetic susceptibility [26]. In our FMR absorption measurements, H is modulated so that the
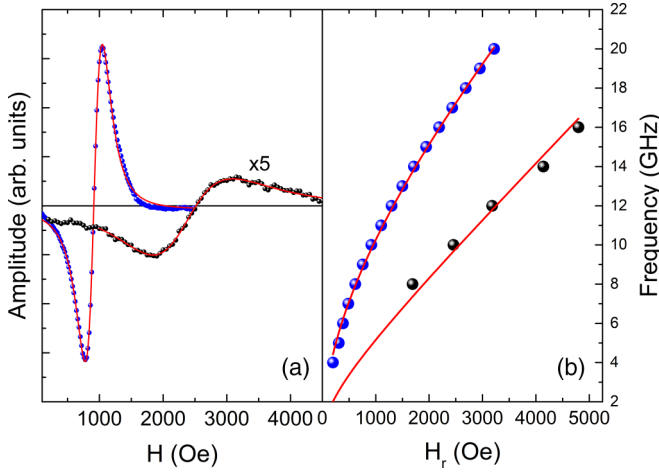
FIG. 5. (a) FMR absorption measurement at 10 GHz for the as-grown (black data points) and annealed (blue) films. (b) Kittel curves (frequency vs resonant field) for the as-grown (black) and annealed (blue) films.

measured signal can be represented by the derivative of the asymmetric Lorentzian with respect to H such that

$$\frac{dP}{dH} = C \frac{-(H - H_R)\Delta H \cos\varepsilon - [(\Delta H/2)^2 - (H - H_R)^2]\sin\varepsilon}{[(\Delta H/2)^2 + (H - H_R)^2]^2}, \tag{3}$$

where C is a constant, H is the applied field, H_R is the resonant field, $\Delta H/2$ is the linewidth corresponding to the HWHM of the Lorentzian, and ε is the phase that mixes real and imaginary parts of the susceptibility. For $\varepsilon = 0°$, the line shape is purely due to the imaginary part of the susceptibility.

The experimental data (symbols) in Fig. 4(a), measured at 10 GHz, are fitted using Eq. (3) (lines). For both films, $\varepsilon \approx 0°$. Resonance for the as-grown film occurs at a bias field of 2370 Oe and displays a relatively large linewidth ΔH, defined as the peak-to-peak width multiplied by $\sqrt{3}/2$, of 1060 Oe. The annealed film shows a stronger resonant amplitude ($\approx 30\times$), a resonance at a lower bias field, 920 Oe, and a narrower linewidth ($\Delta H \approx 230$ Oe). The reduction in both the resonance field and the linewidth correlate to an improved magnetic structure. Resonant fields were extracted for each driving frequency and are plotted in Fig. 5(b) for the as-grown and annealed films.

The data for the annealed sample were fitted using the Kittel equation [27] for a (111) surface and applied fields along the easy axis ($\phi = 0°$),

$$f = \frac{\gamma}{2\pi}\left[\left(H + 2\frac{K_{u\|}}{M}\cos(2\phi)\right)\left(H - \frac{K_1}{M} + \frac{K_{u\|}}{M}(1 + \cos(2\phi))\right.\right.$$
$$\left.\left. + 4\pi M_{\text{eff}}\right) - 2\frac{K_1^2}{M^2}\sin^2(3\phi)\right]^{1/2}, \tag{4}$$

where K_1 and $K_{u\|}$ are the bulk cubic and in-plane uniaxial magnetocrystalline anisotropy constants, respectively, ϕ is the azimuthal angle (in-plane) between the magnetization (field) direction and the anisotropy axis (which is simplified as both K_1 and $K_{u\|}$ have a common axis), and $4\pi M_{\text{eff}} = 4\pi M - 2K_{u\perp}/M$, where $K_{u\perp}$ is the out-of-plane uniaxial anisotropy constant. The g-factor is obtained via the definition

of the gyromagnetic ratio $\gamma = ge/2m$. For the annealed film, a g-factor of 2.19 ± 0.01 is obtained, in good agreement with the value obtained via XMCD and in Ref. [22]. Fits to the FMR data for the annealed film give a large out-of-plane uniaxial anisotropy constant (-8.8×10^5 erg/cm^3). Such a large anisotropy has been reported before [28,29], but the physical origin was not determined. We provide evidence that such a large perpendicular anisotropy is magnetoelastic in origin. The magnetoelastic contribution to the magnetic free energy along the [111] direction is given by

$$f_{\text{ME}} = 3\lambda_{111}c_{44}\varepsilon_{111}\sin^2\theta = K_{\text{ME}}\sin^2\theta, \tag{5}$$

where λ_{111} is the saturation magnetostriction along the $\langle 111 \rangle$ directions, c_{44} is the relevant elastic constant, ε_{111} is the strain along the out-of-plane [111] axis, and θ is the angle the magnetization makes with the strain axis. From the literature, we obtain $\lambda_{111} \approx 90 \times 10^{-6}$ and $c_{44} \approx 7 \times 10^{11}$ dyn/cm^2 [30,31] for Fe$_3$O$_4$. From the XRD data we measure a strain of -0.49% in the out-of-plane direction for the annealed sample, which then gives $K_{\text{ME}} = -9.3 \times 10^5$ erg/cm^3, which is close to the value extracted from the fits to the FMR data for $K_{u\perp}$. Using the extracted values for the anisotropy constants, magnetization, g-factor, and Eq. (4), we generate the in-plane resonance field for a fixed frequency of 10 GHz, which is plotted as the solid line in Fig. 4(b). As can be seen, the simulated curve is in good agreement with the experimental data, indicating we have captured all the pertinent contributions to the magnetic free-energy density. Fits to the frequency field data for the as-grown sample have been performed assuming a cubiclike free energy with the [001] axis perpendicular to the film plane, in contradiction to the XRD data. Therefore, we do not provide details of the fitting parameters, as our free-energy model is inaccurate. However, from the experimental data we observe that the g-factor is reduced compared to the annealed film, consistent with the XMCD.

We note that Kittel's original derivation of the spectroscopic g-factor [Eq. (1)] [18] may require modification so as to include the spin mixing of the valence-band states [32]. Shaw et al. [32] demonstrated a discrepancy between the g-factor obtained from FMR and XMCD for a CoFe/Ni multilayer and Py film, which they account for by including the second-order spin-mixing parameter, b^2, in Eq. (1). While the authors note a large difference in the uncorrected ratio of the orbital to spin moment as measured by FMR and XMCD for Ni, the difference between the two techniques for the uncorrected moment ratio of Fe is much smaller, suggesting a reduced spin-mixing parameter. As the spin-mixing parameter is a consequence of spin-orbit coupling, the effect will also be minimized in materials containing d^5 ions [33]. We therefore expect the correction to the g-factor due to second-order spin-mixing terms to be small for Fe$_3$O$_4$, and well within our experimental uncertainty. Therefore, we do not include such effects in the analysis.

From the static magnetic data, it is evident that annealing the sample in CO/CO$_2$ has improved the magnetic properties of the Fe$_3$O$_4$ thin films. Intuitively, we would therefore also expect the dynamic properties of the film, such as the magnetic damping, to be improved commensurately. However, care must be taken; the larger orbital moment of the annealed film may give rise to enhanced Gilbert damping, as
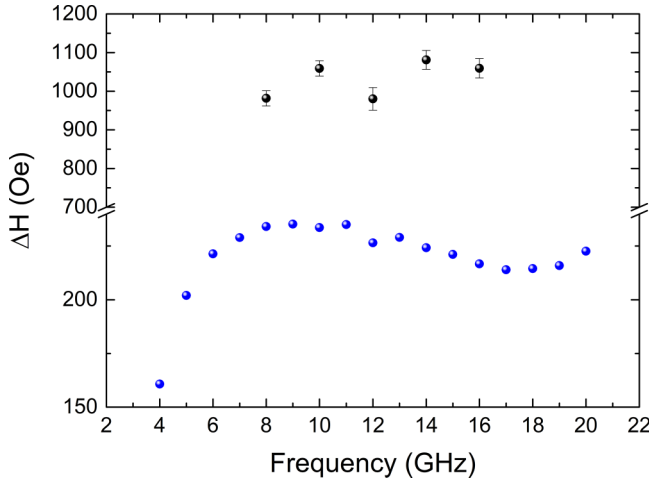
FIG. 6. FMR linewidth (ΔH) vs frequency for the as-grown (black) and annealed (blue) Fe_3O_4 films.

FIG. 7. Magnetic free-energy density plotted as a function of the polar (θ) and azimuthal angle (ϕ) for Fe_3O_4.

was shown by Hrabec *et al.* [34]. Complementary to obtaining the resonant fields as a function of frequency, fits to the field swept FMR data enable the frequency-dependent linewidth (ΔH) to be extracted. Figure 6 shows the field linewidth versus frequency for the as-grown and annealed samples, respectively.

For the as-grown sample, the linewidth is broad (≈ 1000 Oe) and relatively insensitive to frequency. Due to the broad linewidth, data could not be obtained below an FMR frequency of 8 GHz. The flat response of ΔH to frequency is indicative of extrinsic damping due to magnetic inhomogeneities or mixed magnetic phases within the sample. The field linewidth is attributed to a summation of broadening mechanisms [35],

$$\Delta H = \Delta H_0 + \Delta H_{TMS} + \Delta H_{int} = \Delta H_0 + \Delta H_{TMS} + \frac{2\pi\alpha}{\gamma}f,$$
(6)

where f is the microwave frequency, and α is the dimensionless Gilbert damping parameter. The different frequency dependence of these contributions allows for determination of the dominant relaxation mechanism in the sample. While the intrinsic Gilbert damping (ΔH_{int}) shows a linear frequency dependence, magnetic inhomogeneities can lead to a linewidth offset (ΔH_0) and two-magnon scattering (ΔH_{TMS}). Two-magnon scattering contributions scale nonlinearly with microwave frequency, saturating at high frequencies and presenting a steep increase at lower frequencies [36]. The resulting FMR linewidth (ΔH) is the sum of these contributions. For the annealed sample, the linewidth versus frequency data show a characteristic two-magnon scattering line shape, again indicating magnetic inhomogeneities, or mixed magnetic phases, within the sample but with a much reduced linewidth compared to the as-grown sample. However, after the steep increase at low frequencies, the linewidth not only levels off at higher frequencies but it decreases slightly before again increasing after 17 GHz. The consequence of this is a broad peak in $\Delta H(f)$. This profile is not expected from a simplistic view of magnetic relaxation in which the linewidth should always increase with frequency, as shown in Eq. (5).
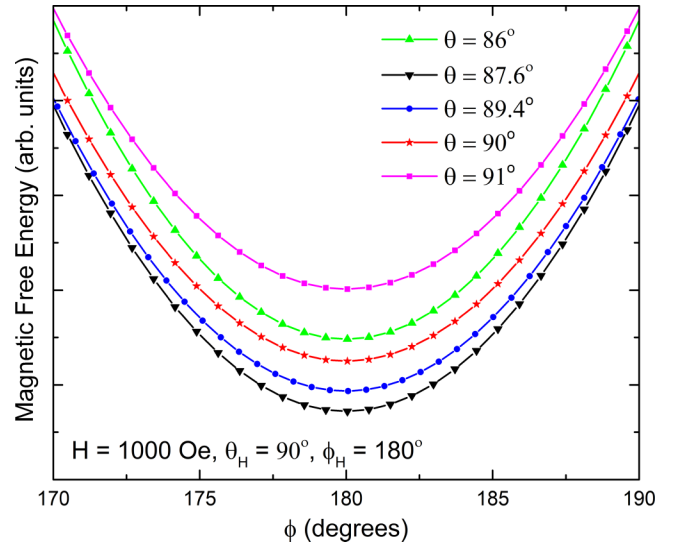
Such a profile is observed in spherical samples in which the "Buffler" peak [37], due to the band-edge crossover effect, is the signature for grain-to-grain two-magnon scattering. The Buffler peak is a purely geometric effect that, despite being present in spherical samples, should not be observed in thin films. Landeros *et al.* [38] show a similar feature in calculations of the FMR linewidth due to two-magnon scattering when there is a small tipping angle ($\approx 5°$) between the magnetization and film plane. The nonmonotonic behavior of the linewidth with frequency at these angles is similar in shape to our experimental data. In [38] the angle is kept constant as a function of frequency, which is not possible experimentally due to the increasing in-plane H field with frequency. However, this would smooth out the effect for modest changes in the polar angle of the magnetization, and the effect is visible over a broad range of polar angles. Only when M is exactly in-plane does the linewidth with frequency show monotonic behavior. Calculating the magnetic free-energy density (F) for the (111) orientation of Fe_3O_4, including the magnetocrystalline anisotropy energy, the demagnetization energy, and Zeeman energy for an in-plane field of 1000 Oe ($\theta_H = 90°$, $\phi_H = 180°$), we find that the free energy is minimized ($\partial F/\partial\theta = 0$, $\partial F/\partial\phi = 0$) when the magnetization is tilted marginally out of plane by $\approx 2°$, as shown in Fig. 7.

According to Ref. [38], this small tilting angle would give rise to the observed nonmonotonic behavior in the FMR linewidth with frequency consistent with our data.

IV. SUMMARY

Thin-film Fe_3O_4 was grown on YSZ(111) substrates using PLD. High-temperature (1100 °C) annealing in a reducing atmosphere allows bulklike structural and magnetic properties to be recovered without significant film substrate intermixing. An unusual fourfold magnetic anisotropy is observed for the as-grown films that transforms to the expected sixfold symmetry of the (111) surface upon annealing. A finite orbital

moment was measured using XMCD and FMR, in agreement with recent hard x-ray measurements, adding further evidence to a long-standing and contentious debate concerning this quantity. While bulklike static magnetic properties are recovered upon annealing, the high-frequency dynamic properties are still dominated by two-magnon scattering and a nonmonotonic behavior observed in the field linewidth as a function of frequency, in agreement with the predictions of Landeros *et al.* [38].

ACKNOWLEDGMENT

[1] C. Fesler, G. H. Fecher, and B. Balke, Angew. Chem. **46**, 668 (2007).

[2] W. Eerenstein, T. T. M. Palstra, S. S. Saxena, and T. Hibma, Phys. Rev. Lett. **88**, 247204 (2002).

[3] K. P. McKenna, F. Hofer, D. Gilks, V. K. Lazarov, C. Chen, Z. Wang, and Y. Ikuhara., Nat. Commun. **5**, 5740 (2014).

[4] J. B. Goodenough, J. Phys. Chem. Solids **6**, 287 (1958). J. Kanamori., **10**, 87 (1959).

[5] W. Erenstein, T. T. M. Palstra, T. Hibna, and S. Celotto, Phys. Rev. B **66**, 201101(R) (2002).

[6] E. Liu, Y. Yin, L. Sun, Y. Zhai, J. Du, F. Xu, and H. Zhai, Appl. Phys. Lett. **110**, 142402 (2017).

[7] D. Gilks, L. Lari, K. Matsuzaki, H. Hosono, T. Susaki, and V. K. Lazarov, J. Appl. Phys. **115**, 17C107 (2014).

[8] S. S. Kalarickal, N. Mo, P. Krivosik, and C. E. Patton, Phys. Rev. B **79**, 094427 (2009).

[9] C. J. Love, B. Kuerbanjiang, A. Kerrigan, S. Yamada, K. Hamaya, G. van der Laan, V. K. Lazarov, and S. A. Cavill, Appl. Phys. Lett. **119**, 172404 (2021).

[10] B. Kuerbanjiang, C. Love, D. Kepaptsoglou, Z. Nedelkoski, S. Yamada, A. Ghasemi, Q. M. Ramasse, K. Hamaya, S. A. Cavill, and V. K. Lazarov, J. Alloys Compd. **748**, 323 (2018).

[11] S. S. Dhesi, S. A. Cavill, A. Potenza, H. Marchetto, R. A. Mott, P. Steadman, A. Peach, E. L. Shepherd, X. Ren, U. H. Wagner, and R. Reininger, AIP Conf. Proc. No. 1234 (AIP, New York, 2010), p. 311.

[12] E. J. Verwey, Nature (London) **144**, 327 (1939). X. Liu, C-F. Chang, A. D. Rata, A. C. Komarek, and L. H. Tjeng, npj Quantum Mater. **1**, 16027 (2016).

[13] G. van der Laan and A. I. Figueroa, Coord. Chem. Rev. **277**, 95 (2014).

[14] R. Nakajima, J. Stohr, and Y. U. Idzerda, Phys. Rev. B **59**, 6421 (1999).

[15] P. Morrall, F. Schedin, G. S. Case, M. F. Thomas, E. Dudzik, G. van der Laan, and G. Thornton, Phys. Rev. B **67**, 214408 (2003).

[16] G. van der Laan and B. T. Thole, Phys. Rev. B **43**, 13401 (1991). E. Stavitski and F. M. F. de Groot, Micron **41**, 687 (2010).

[17] B. T. Thole, P. Carra, F. Sette, and G. van der Laan, Phys. Rev. Lett. **68**, 1943 (1992); C. T. Chen, Y. U. Idzerda, H.-J. Lin, N. V. Smith, G. Meigs, E. Chaban, G. H. Ho, E. Pellegrin, and F. Sette., **75**, 152 (1995).

[18] C. Kittel., Phys. Rev. **76**, 743 (1949).

[19] E. Goering, S. Gold, M. Lafkioti, and G. Schutz, Europhys. Lett. **73**, 97 (2005).

[20] D. J. Huang, C. F. Chang, H.-T. Jeng, G. Y. Guo, H.-J. Lin, W. B. Wu, H. C. Ku, A. Fujimori, Y. Takahashi, and C. T. Chen, Phys. Rev. Lett. **93**, 077204 (2004).

[21] E. Goering, Phys. Status Solidi B **248**, 2345 (2011).

[22] H. Elnaggar, Ph. Sainctavit, A. Juhin, S. Lafuerza, F. Wilhelm, A. Rogalev, M.-A. Arrio, Ch. Brouder, M. van der Linden, Z. Kakol, M. Sikora, M. W. Haverkort, P. Glatzel, and F. M. F. de Groot, Phys. Rev. Lett. **123**, 207201 (2019).

[23] L. R. Bickford, Phys. Rev. **78**, 449 (1950).

[24] S. M. Rezende, J. A. S. Moura, F. M. de Aguiar and W. H. Schreiner, Phys. Rev. B **49**, 15105 (1994).

[25] H-F. Du, W. He, H-L. Liu, Y-P. Fang, Q. Wu, T. Zou, X-Q. Zhang, Y. Sun, and Z-H. Cheng, Appl. Phys. Lett. **96**, 142511 (2010).

[26] D. E. Parkes, L. R. Shelford, P. Wadley, V. Holý, M. Wang, A. T. Hindmarch, G. van der Laan, R. P. Campion, K. W. Edmonds, S. A. Cavill, and A. W. Rushforth., Sci. Rep. **3**, 2220 (2013).

[27] J. Smit and H. G. Beljers, Philips Res. Rep. **10**, 113 (1955); G. Gubbiotti, G. Carlotti, and B. Hillebrands, J. Phys.: Condens. Matter **10**, 2171 (1998).

[28] Y. Zhai, Z. C. Huang, Y. Fu, C. Ni, Y. X. Lu, Y. B. Xu, J. Wu, and H. R. Zhai, J. Appl. Phys. **101**, 09D126 (2007).

[29] Z. C. Huang, X. F. Hu, Y. X. Xu, Y. Zhai, Y. B. Xu, J. Wu, and H. R. Zhai, J. Appl. Phys. **111**, 07C108 (2012).

[30] L. R. Bickford, J. Pappis, and J. L. Stull, Phys. Rev. **99**, 1210 (1955).

[31] T. J. Moran and B. Luth, Phys. Rev. **187**, 710 (1969).

[32] J. M. Shaw, R. Knut, A. Armstrong, S. Bhandary, Y. Kvashnin, D. Thonig, E. K. Delczeg-Czirjak, O. Karis, T. J. Silva, E. Weschke, H. T. Nembach, O. Eriksson, and D. A. Arena, Phys. Rev. Lett. **127**, 207201 (2021).

[33] D. Cheshire, P. Bencok, D. Gianolio, G. Cibin, V. K. Lazarov, G. van der Laan, and S. A. Cavill, J. Appl. Phys. **132**, 103902 (2022).

[34] A. Hrabec, F. J. T. Gonçalves, C. S. Spencer, E. Arenholz, A. T. N'Diaye, R. L. Stamps, and C. H. Marrows, Phys. Rev. B **93**, 014432 (2016).

[35] G. Woltersdorf and B. Heinrich, Phys. Rev. B **69**, 184417 (2004).

[36] R. Arias and D. L. Mills, Phys. Rev. B **60**, 7395 (1999).

[37] C. R. Buffler, J. Appl. Phys. **30**, S172 (1959).

[38] P. Landeros, R. E. Arias, and D. L. Mills, Phys. Rev. B **77**, 214405 (2008).